International Journal of Refractory Metals and Hard Materials 113 (2023) 106187

Contents lists available at ScienceDirect

International Journal of Refractory Metals and Hard Materials

journal homepage: www.elsevier.com/locate/IJRMHM

Improved adhesion of cathodic arc PVD AlCrSiN coating on ion-implanted WC-Co substrates

L. Ortiz-Membrado [a,*], S. García-González [a], J. Orrit-Prat [c], R. Bonet [c], J. Caro [c], J. Fernández de Ara [d], E. Almandoz [d,e], L. Llanes [a,b], E. Jiménez-Piqué [a,b]

[a] CIEFMA – Department of Materials Science and Engineering, EEBE, Universitat Politècnica de Catalunya-BarcelonaTECH, Avda. Eduard Maristany 16, 08019 Barcelona, Spain
[b] Barcelona Research Center in Multiscale Science and Engineering, Universitat Politècnica de Catalunya-BarcelonaTECH, Avda. Eduard Maristany 16, 08019 Barcelona, Spain
[c] Eurecat, Centre Tecnològic de Catalunya, Unit of Metallic and Ceramic Materials, Plaça de la Ciència 2, 08243 Manresa, Spain.
[d] Centre of Advanced Surface Engineering, AIN, 31191 Cordovilla, Spain
[e] Science Department, Universidad Pública de Navarra (UPNA), Campus de Arrosadía, 31006 Pamplona, Spain

ARTICLE INFO

Keywords:
Ion implantation
AlCrSiN
PVD coatings
Residual stresses
Hardmetals

ABSTRACT

Ion implantation has been shown to improve adhesion strength of AlCrSiN coatings due to a synergic enhancement on fracture toughness and load bearing capability of the substrate that can potentially increase the in-service efficiency of coated cutting tools. In this work, AlCrSiN coatings deposited by PVD on WC-Co substrates implanted with Ti, Cr and N ion species have been processed. The mechanical properties and adhesion have been characterized by contact techniques and the residual stress of the coatings and substrates have been evaluated using FIB-DIC technique and Vickers indentation tests, respectively. An improvement of adhesion strength is obtained for treated substrates, especially for those implanted with titanium and chromium ions. This improvement is attributed to the introduction of residual stresses in the substrate, which increases its fracture toughness and enhances its load bearing capability.

1. Introduction

The process of cutting metals, which includes a broad range of methods for shaping metals such as milling, turning, drilling and particularly high speed cutting, generates large mechanical forces and high temperatures at the contact point between the cutting tool and the workpiece material [1]. Cemented carbides, also referred as hardmetals, are materials increasingly used because of their high hardness, wear-resistance and fracture strength, with also a good fracture toughness, prolonging the service life and reliability for machining operations. To enhance their performance, cutting tools are often protected by coatings designed to increase hardness, wear resistance and corrosion resistance [2–6]. Metal nitride coatings, such as CrAlSiN and other combinations [7], had attracted increasing interest due to their improved properties including exceeding hardness, resistance against high-temperature oxidation, low friction, and outstanding thermal stability.

Although hardness, and thus wear resistance, is an important property for coatings in cutting tools, good adhesion and toughness are capital under impact conditions to avoid premature failure of the tool. However, super-hard ceramic coatings are usually related to low fracture toughness and lower adhesion to the substrate. In particular, some results have shown that AlCrN-based coatings exhibit weak adhesion during scratch and impact tests [8–10]. Different methods have been developed to obtain coatings with enhanced hardness and toughness and improved adhesion strength, from the creation of a gradient structure [11], satisfying the requirements of the coating throughout the coating thickness, to a multilayer structure [12], including crack deflection mechanisms [13,14].

Other methods that focus on the substrate-coating cohesion can be an alternative approach to improve adhesion without changing mechanical and thermal properties, introducing compressive residual stresses to the coating and substrate. Some ways to introduce residual stress are, for instance, with different bias voltages via sputtering [15,16], by phase change [17] or by ion implantation [18].

High-dose ion implantation has been used to introduce surface residual stresses, modifying the surface chemical and mechanical

* Corresponding author.
E-mail address: laia.ortiz@upc.edu (L. Ortiz-Membrado).

https://doi.org/10.1016/j.ijrmhm.2023.106187
Received 7 October 2022; Received in revised form 6 March 2023; Accepted 8 March 2023
Available online 11 March 2023
0263-4368/© 2023 The Authors. Published by Elsevier Ltd. This is an open access article under the CC BY-NC-ND license (http://creativecommons.org/licenses/by-nc-nd/4.0/).

properties of materials, as observed by Halitim et al. [18]. The effect that the ion implantation of the substrate with different types of ions has on the coating adhesive properties has been a focus of interest, with a significant improvement in the mechanical properties and adhesion of the coatings [19–23].

Ion implantation proves to be effective in improving the adhesion of hard coatings. However, related studies concerning the influence of ion implantation on the adhesion strength of protective hard coatings are quite limited for hardmetal substrates. In this paper, the adhesion of AlCrSiN coatings to WC-Co substrates with Ti, Cr, and N implantation using Plasma Immersion Ion Implantation (PIII) has been compared by means of scratch and Mercedes tests, as well as by the subsequent FIB-SEM inspection of the formed scratch cracks. Results have been correlated with fracture toughness of the substrate and residual stress of the coating.

2. Materials and methods

2.1. Materials

A WC-Co hardmetal, with 0.9 ± 0.4 μm of grain size and 10% of cobalt content, coated with an AlCrSiN PVD layer was selected for this study. Four different substrates were studied in this work: reference substrate without ion implantation, and three substrates with nitrogen, titanium and chromium implantation. AlCrSiN coating was subsequently deposited on these samples, as it is schematically depicted in Fig. 1. Prior to deposition and implantation, substrates were mirror polished.

Ti, Cr and N were implanted in hardmetal samples by means of Plasma Immersion Ion Implantation (PIII) technique. Ti and Cr cathodes (99.9% purity) were evaporated using a pulsed filtered cathodic arc source synchronized with a high voltage bias power supply (PFCA-450, Plasma Technology Limited). For N implantation, N_2 gas flow of 20 sccm was introduced into the vacuum chamber through an End-Hall ion source while biasing the substrates to a high negative voltage. In all the processes, the vacuum chamber was preheated for desorption of any possible contaminant and evacuated to a pressure below $5{\cdot}10^{-3}$ Pa. The initial temperature was around 50 °C and treatment time was 60 min. The main ion implantation parameters are summarized in Table 1. Taking into account that sample holder area was 20 cm^2, incident ion dose was estimated to be $1.1{\cdot}10^{18}$ ions/cm^2 for titanium and chromium, and $2.5{\cdot}10^{18}$ ions/cm^2 for nitrogen.

Cathodic arc evaporation was used to deposit the 2 μm AlCrSiN coating. The process was carried out using the industrial equipment PLATIT p80 units, in a vacuum chamber with an argon atmosphere at 0.8–2 Pa and a negative bias voltage of −65 V. Incorporating the LARC technology, which is a turnable magnetic field, and using pure Cr at 99.9% and Al + 12%at.Si as material source, a 2 μm single layered nanocomposite AlCrSiN coating is deposited. The technology is explained in more detail by A. Mosquera et al. in [24].

2.2. Microstructural and mechanical characterization

A SEM equipped with FIB (Carl Zeiss Neon40 Crossbeam) operated at 30 kV was used to obtain images and cross sections of the samples.

X-ray photoelectron spectroscopic (PS) measurements on the substrates were performed in a PHI VersaProbe II from Physical Electronics. The source of x-rays was Al (1486.6 eV) monochromatic at 24.9 W, with a beam diameter of 100 μm. The samples were sputtered with 1.0 kV Ar^+ monoatomic, 1 prespputter cycle, 61 sputter cycles, AlternatingZalar sputter mode, with sample rotation and a sputter rate of 3.1 nm/min in SiO_2.

Vickers indentation test was performed to measure hardness (HV) and fracture toughness of the substrates, the latter obtained by Vickers indentation crack length method proposed by Niihara et al. [25,26]. Six indentations were made for each sample at 30 kgf. The generated cracks were measured by optical microscopy.

Residual stress of the substrate was also estimated using Vickers indentation crack length and fracture toughness obtained value, assuming the relation in Eq. (1), where the fracture toughness of the stress free surface (K_{Ic}) is the combination of the fracture toughness of the surface with residual stresses (K_{Ic}^A) and the stress intensity factor due to these stresses (K_I^R):

$$K_{Ic} = K_{Ic}^A + K_I^R \tag{1}$$

Green and Maloney [27] found that for a surface stress to a depth d from the surface, the value K_I^R is given by:

$$K_I^R = \sigma_c Y c^{1/2} \tag{2}$$

where c is the crack length, σ_c the compressive stress in the surface and Y depends on c/d. De Portu and Conoci [28] found that for $c>>>d$ the function Y approaches the limit 0.73. Assuming an ion implantation depth around 100–200 nm, Y approaches this limit and substituting (2) in (1) the stress in the surface can be expressed as:

$$\sigma_c = \frac{K_{Ic} - K_{Ic}^A}{0.73 c^{1/2}} \tag{3}$$

Glow discharge optical emission spectroscopy (GDOES) was used to obtain the chemical composition of the films. The GDOES analyses were performed using a Jovin-Yvon JY 1000 RF optical spectrometer equipped with more than 40 channels and an optical monochromator.

Roughness of the coated samples was measured using the confocal

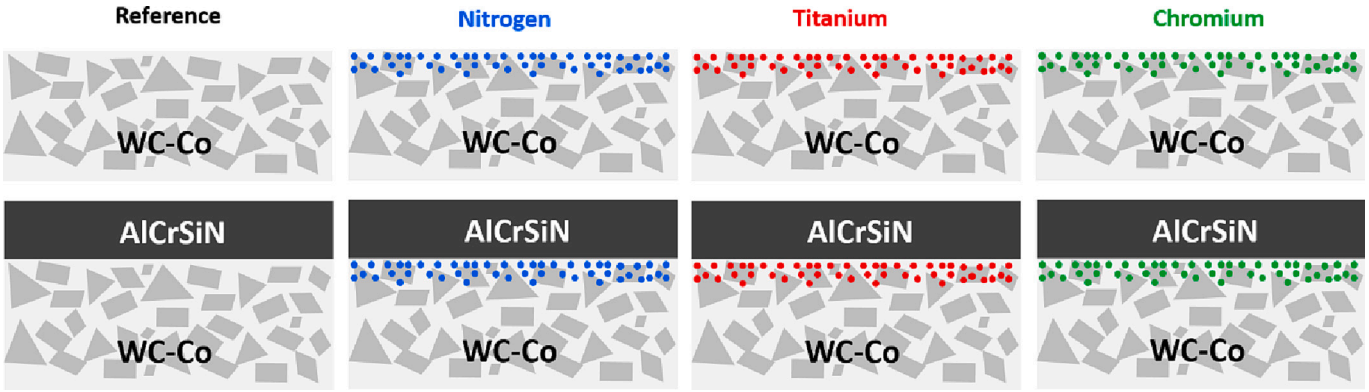

Fig. 1. Schematic representation of the samples of study. From left to right: WC-Co, WC-Co + N, WC-Co + Ti, WC-Co + Cr, AlCrSiN, N/AlCrSiN, Ti/AlCrSiN and Cr/AlCrSiN.

Table 1
Ion implantation process parameters.

Element	Argon Flow (sccm)	Pressure (Pa)	Frequency (Hz)	Pulse Width (μs)	Bias Voltage (kV)	Bias Current (mA)	Final Temperature (°C)
Ti/Cr	2.5	$3.0{\cdot}10^{-2}$	8	600	25	40	280
N_2	–	$2.8{\cdot}10^{-1}$	200	40	25	45	265

microscope Olympus LEXT OLS 3100. Average roughness (R_a) and average maximum height of the profile (R_z) were calculated for each coating. For each sample the analysis was carried out in four different areas of around $100{\cdot}100\mu m^2$.

Hardness and elastic modulus of the coating were analysed by means of nanoindentation using a MTS Nanoindenter XP. A matrix of 5 × 5 indentations, with 50 μm of spacing and a maximum penetration depth of 2000 nm was performed in each coated sample. For the tests, a Berkovich indenter tip calibrated on fused silica reference sample at same conditions was used. Oliver and Pharr method [29] was applied. Hardness and Young's modulus of the coating were deconvoluted from the substrate, measuring the hardness at 10% of the penetration depth, and extrapolating the values of Young's modulus [30].

Residual stress was measured using Digital Image Correlation (DIC) method based on Focus Ion Beam (FIB) milled double slot features [31–35]. In this method, DIC was applied comparing two images: before and after the milling of the selected geometry with FIB. Applied magnification resulted in a pixel size of around 15 nm. Images were taken with samples tilted 54° with tilt correction, and 5 kV of acceleration voltage.

Double slot geometry was used to measure residual stress [36]. Since the thickness of the coating was around 2 μm, the distance between the two slots (d) was chosen to be between 1 and 2 μm. Two slots were milled with 10 μm length (L) and 1 μm width (w) using a current of 500 pA. The depth (h) of the milled slots was equal to the coating thickness (t), since from this point the relaxation strain obtained was maximum and independent from the depth [32].

VIC-2D-software for digital image correlation was used to obtain the real strain field for x-direction in the area between milled slots. An average strain among the area between the slots was calculated, and regions that deviated significantly from the mean were considered as ion beam affected areas and were discarded. This average strain in x-direction was defined as $\Delta\varepsilon^{I}_{xx}$ and residual stress (σ_{res}) was measured using Eq. (4) [34,36].

$$\sigma_R = -\Delta\varepsilon^{I}_{xx}\frac{E}{1-\upsilon^2} \tag{4}$$

Where E is the Young's modulus of the coating, and ν is the Poisson's ratio. The initial and final states from which this equation is obtained are represented in Fig. 2.

For the scratch test, ASTM C1624–05 [37] standard was followed for the determination of test parameters and identification of damage features. An incremental load of 1 to 100 N was applied at a 100 N/min in a distance of 5 mm with a Rockwell C tip (conical diamond indenter with an included angle of 120° and a spherical tip radius of 200 μm). Two critical loads were defined and identified for each coating: L_{c1} as the critical load where arc tensile cracks appear and L_{c2} as the load at which first chipping and substrate exposure is observed. Critical loads were identified using optical microscope. SEM and FIB were used for further evaluation of the failures.

To complement adhesion evaluation and comparison of the different samples, a Mercedes adhesion test was performed [38]. For that, A Rockwell-C indenter was pressed into the surface of the coating with 196 N, 294 N, 392 N and 490 N loads during 10 s. Indents were analysed using optical microscopy to determine and compare the amount of delamination area at different loads between different samples.

3. Results

3.1. Substrate characterization prior to coating deposition

SEM images in Fig. 3 show the surface of the substrate before and after the ion implantation process. After titanium and chromium implantation, etching of the surface is observed in WC grains, while after nitrogen implantation, no significant morphological changes are appreciated. XPS analysis shows that in the Ti, Cr and N implanted samples the maximum profile concentration is 4.5% at. Ti, 1.8% at. Cr and 17% at. N, respectively. The XPS profiles are presented in Fig. 4. The nitrogen concentration is higher, so the substrate implanted with nitrogen has more implanted ions than the substrates implanted with Cr and Ti. This is consistent with Fig. 3, where it is evident that the N-implanted sample has no sputtering on the surface, unlike the Cr- and Ti-implanted samples.

Apparent fracture toughness and hardness of the substrates are presented in Table 2. At the applied load, the indentation penetration depth is uniform for all substrates, the average depth 26.7 ± 0.1 μm, as well as the hardness, which is similar for all the substrates, as presented. Apparent fracture toughness of the sample treated with nitrogen is similar to the reference, while higher values are obtained for samples with Ti and Cr implantation. Also looking at the crack lengths for Cr and Ti implanted samples, the generated cracks are smaller than in the reference substrate, indicating the presence of compressive stresses for these implanted samples [39]. Vickers indentation cracks are presented in Fig. 5. Calculated residual stress of the substrates using Eq. (3) is consistent with the measured crack lengths, indicating the presence of significant compressive stresses for Ti- and Cr- implanted substrates.

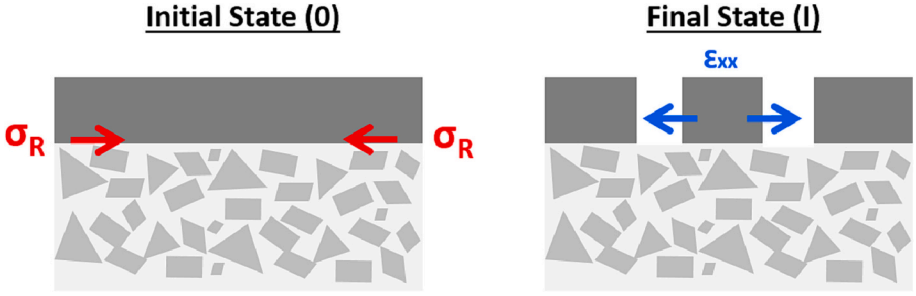

Fig. 2. Illustration representing the initial and final state, before and after the milling of the two slots using FIB. In the initial state an equibiaxial residual stress state is assumed and in the final state, after the milling, a stress relaxation occurs.

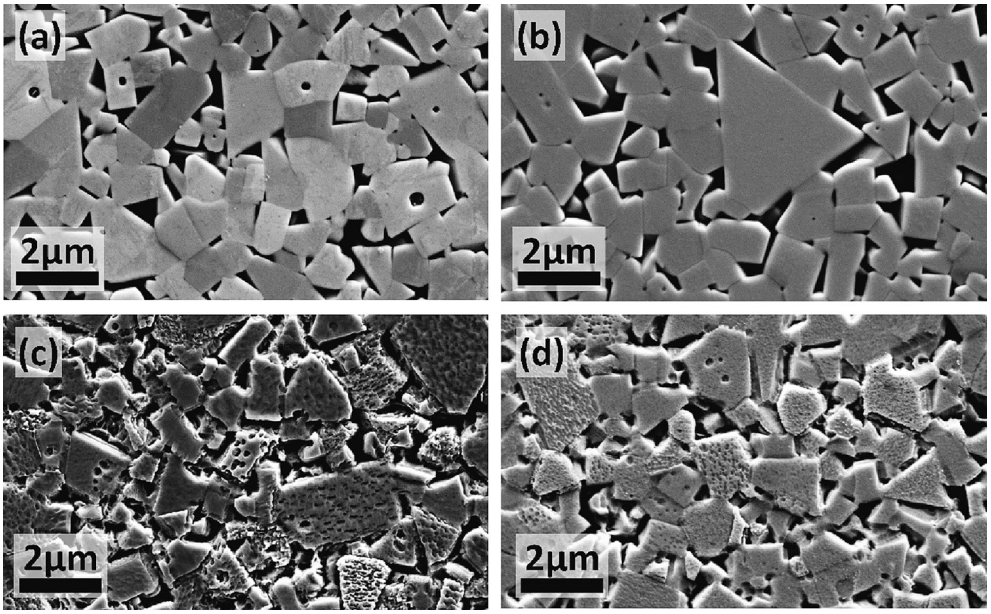

Fig. 3. SEM images of WC-Co substrate before (a) and after ion implantation of: (b) nitrogen, (c) titanium and (d) chromium.

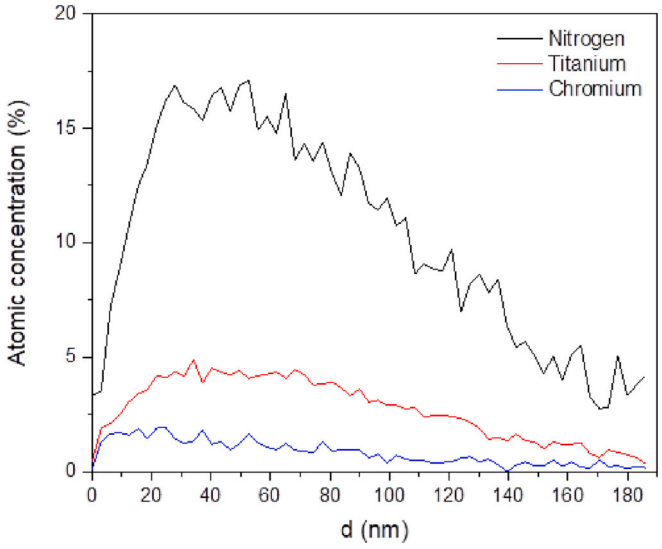

Fig. 4. XPS results of the profiles of the elements implanted on the substrates. Atom concentration as a function of depth (*d*) in nm, taking into account the sputter rate of 3.1 nm/min obtained on a SiO_2 standard sample.

Table 2
Hardness, apparent fracture toughness, length of the Palmqvist cracks (c) and residual stress of the substrates.

	WC-Co	WC-Co + N	WC-Co + Ti	WC-Co + Cr
Hardness [GPa]	15.5 ± 0.1	15.6 ± 0.1	15.7 ± 0.2	15.7 ± 0.2
K_{Ic} [MPa·m$^{1/2}$]	12.7 ± 0.1	12.5 ± 0.9	15.4 ± 1.4	17.1 ± 2.4
c [µm]	87.5 ± 0.5	90.3 ± 13.5	60.8 ± 10.9	50.2 ± 13.3
σ_c [MPa]	–	29 ± 122	−472 ± 236	−846 ± 452

3.2. Coating characterization

Fig. 6 shows the atomic composition as a function of depth for the reference non implanted coated sample. The approximate chemical composition of the coating is $Cr_{0.60}Al_{0.30}Si_{0.04}N$, where the (Cr + Al + Si)/N ratio is 1.3. Also, an adhesion metallic Cr layer, consequence of the deposition technology, could be observed since the chromium content is higher at the coating-substrate interface.

Elastic modulus and hardness as a function of penetration depth were obtained using nanoindentation test for coated samples. Values reach a plateau for penetration depths from 800 nm, where curves tend to the substrate values. Hardness and elastic modulus of the coated samples were similar for implanted and reference samples, around 30 GPa and 400 GPa, respectively.

All coated samples presented a similar surface morphology typical of arc deposition PVD, but measured average roughness values, presented in Table 3, show that higher average roughness is obtained for ion-implanted-substrate samples.

Cross-sectional SEM images of the four samples were carried out. Thickness of the coatings was found to be around 2 µm and typical column structure was discerned (Fig. 7).

3.3. FIB-DIC residual stress measurement

FIB-DIC technique was carried out for all samples. Fig. 8 shows a SEM image after the milling of double slot geometry for Cr/AlCrSiN sample, and x-direction strain field ($\mathcal{E}_{xx}$) calculated by DIC. Poisson's ratio and elastic modulus were assumed 0.25 and 400 GPa, respectively, used to calculate the average residual stress using Eq. (4).

Results of strain and residual stresses in *x*-direction using FIB-DIC technique for the coated samples are presented in Table 4. Similar values of compressive residual stress were obtained for all the coatings. The same technique was applied to measure residual stress of the reference substrate, with no ion implantation. No deformation was detected, therefore residual stress was zero, as expected.

3.4. Adhesion

In Fig. 9 the scratch track of each sample is presented with the corresponding location of critical loads (L_c) for the first appearance of specific failures related to scratch resistance and adhesion of coatings. L_{c1}, when first arc tensile cracks appear, is associated with cohesive failure of the coating, and it is not largely affected by the ion implantation of the substrate. L_{c1} was found similar for all the coatings, around 50 N. The main difference between the coatings is with the L_{c2}, when first chipping or spallation occurs and the substrate is exposed,

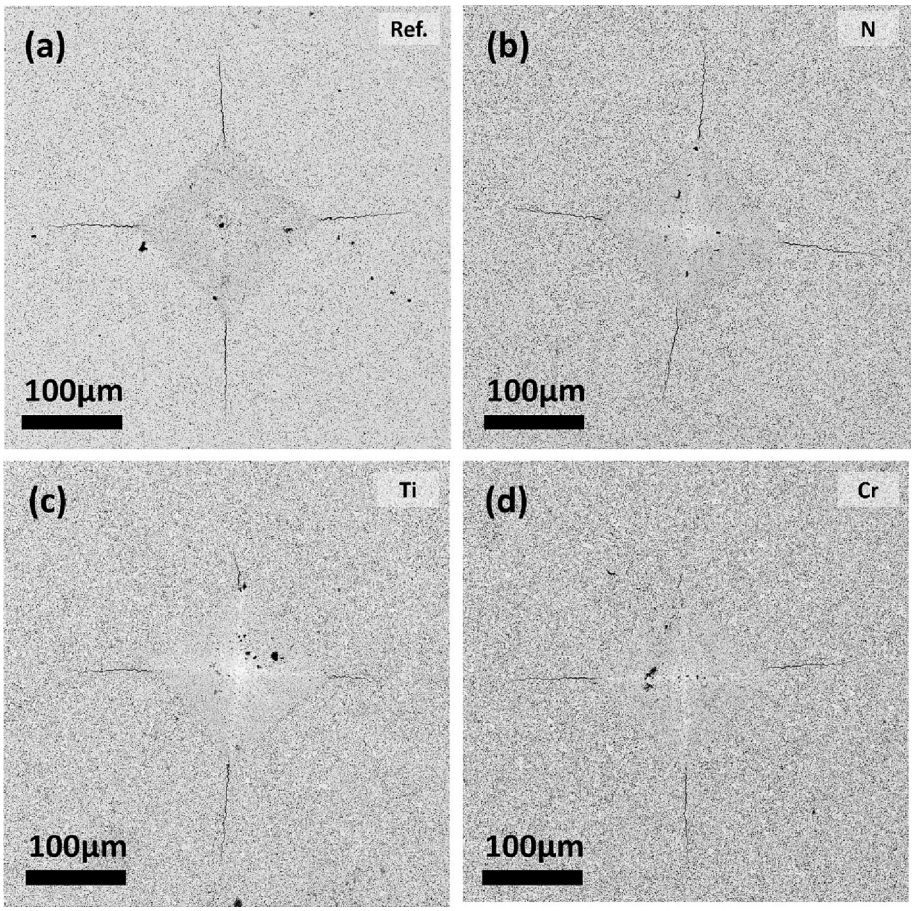

Fig. 5. SEM images showing cracks emanated from Vickers indentations of: (a) WC-Co reference substrate and (b) nitrogen, (c) titanium and (d) chromium implanted samples. Ti- and Cr implanted samples present smaller cracks than the reference, indicating the presence of compressive stresses.

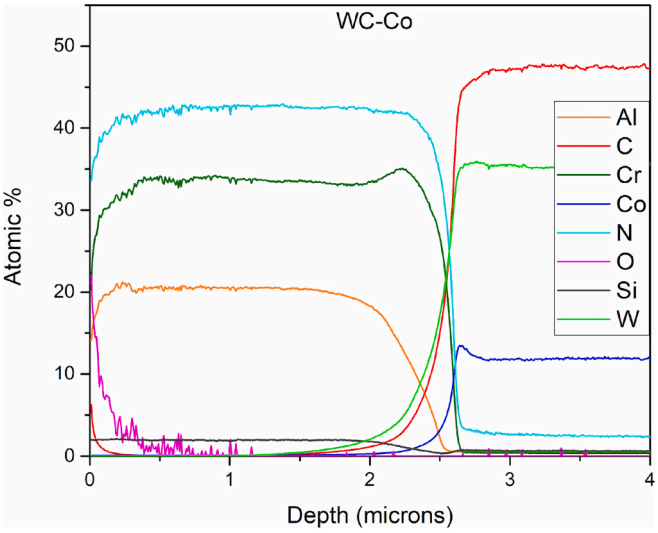

Fig. 6. Linescan of the chemical composiition of AlCrSiN coating carried out using GD-OES technique.

Table 3
Average roughness (Ra) and maximum peak height(Rz) of the coatings.

	Ref. AlCrSiN	Ti/AlCrSiN	Cr/AlCrSiN	N/AlCrSiN
R_a (µm)	0.057 ± 0.010	0.082 ± 0.010	0.082 ± 0.003	0.097 ± 0.008
R_z (µm)	3.0 ± 0.3	3.0 ± 0.3	5.5 ± 0.4	5.1 ± 0.6

indicating adhesive failure. It can be clearly observed that ion-implanted samples show better adhesive strength, while the reference coating presents a large area of spallation and the defect appears at lower loads. For the reference, coating spallation with substrate exposure starts at 70 N, while for implanted samples it appears between 80 and 85 N. Analysing the spallation area with SEM images in Fig. 10, for both reference and nitrogen implanted sample, more substrate exposure is observed, which corresponds to whiter areas, while in titanium and chromium implanted samples less coating area is lifted exposing the substrate, indicating a better adhesive strength.

To visualize the deformation and fracture mechanisms, cross-sectional SEM images were taken at the same load, 80 N, for all samples (Fig. 11). It can be observed that in the reference coating and the N-implanted sample the crack goes through the coating and fractures the carbides as well. However, for Cr- and Ti- implanted samples there is no apparent fracture in the carbides.

Observing the images of the spallation area it can be seen that at 80 N in reference coating and the nitrogen implanted sample the substrate exposure area is very extended and carbides are clearly exposed, while, at 90 N, in the Ti and Cr samples some coating still remains attached to the carbides. In all images of scratch test failures of titanium implanted sample, less carbides are exposed, therefore titanium provides the coating with better adhesion.

Finally, Mercedes test was performed for all samples at different loads. Optical images of the indentations are presented in Fig. 12. At 147 N no delamination can be observed for any of the coatings. At 196 N first delamination occurs for reference, nitrogen and titanium implanted samples, with the titanium-implanted one showing lower delamination

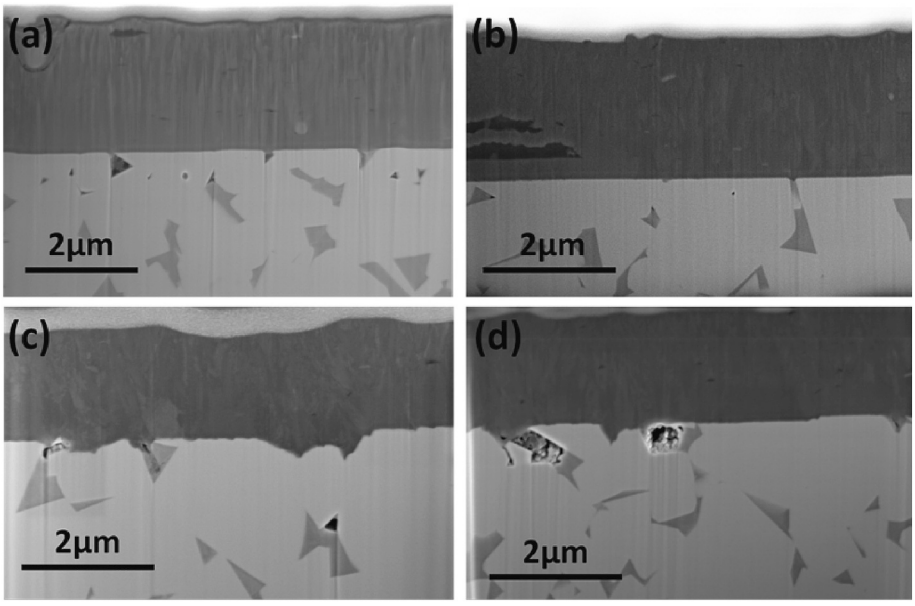

Fig. 7. Cross-sectional SEM images of: (a) Reference AlCrSiN, (b) N/AlCrSiN, (c) Ti/AlCrSiN and (d) Cr/AlCrSiN.

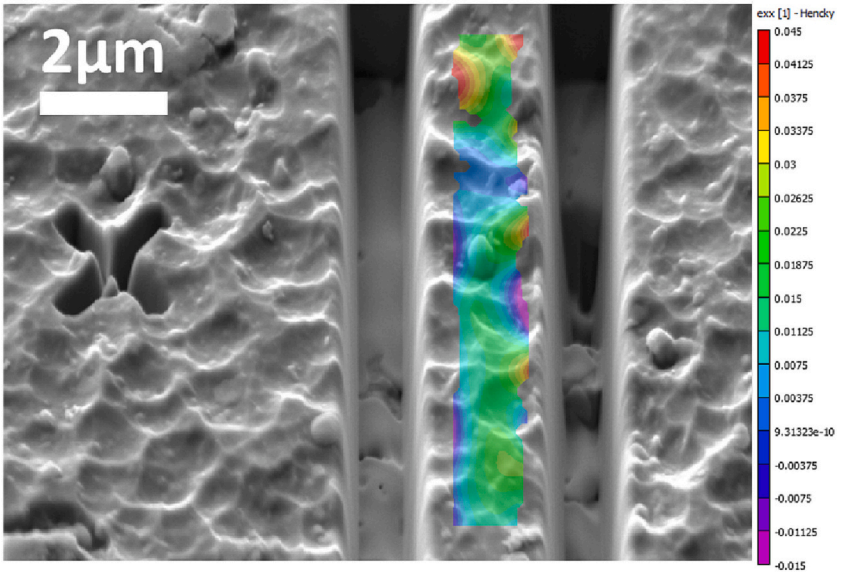

Fig. 8. SEM image after double slot milling, with DIC strain field obtained for Cr/AlCrSiN.

Table 4
Residual stresses calculated using FIB-DIC technique.

Sample	Ref. AlCrSiN	N/AlCrSiN	Ti/AlCrSiN	Cr/AlCrSiN
$\Delta\varepsilon xx$ ($x10^{-3}$)	14 ± 6	14 ± 9	13 ± 2	16 ± 6
Residual Stress (GPa)	−5.9 ± 2.5	−5.8 ± 3.8	−5.7 ± 0.6	−6.6 ± 2.7

area. At this load, the chromium-implanted sample shows no delamination. At higher loads the non-implanted sample has the larger delamination area, while titanium and chromium samples present less delamination area, which is consistent with the scratch test results. Substrate exposure area was measured with an image processing program. At 196 N the substrate exposure is $4.2{\cdot}10^3$, $1.1{\cdot}10^3$ and $0.2{\cdot}10^3$ μm^2 for AlCrSiN, N/AlCrSiN and Ti/AlCrSiN, respectively, and for Cr/AlCrSiN there is no substrate exposure.

4. Discussion

The surface morphology caused by sputtering or etching observed in Cr and Ti implanted samples is related to the atomic mass of the atoms (Ti: 47,9 g/mol, Cr: 52 g/mol, N: 14 g/mol). The rate of sputtering depends on the incident ion mass and energy and the substrate material. In this case, it is evident that the differential factor is the mass of the incident ion: for Ti and Cr, it is much higher than that of N, causing more sputtering and modifying the surface of the substrate. As it can be seen in Fig. 3, the sample with titanium implantation presents grains with more sputtering than others. As it is well known, WC has a hexagonal structure and the orientation of the grains may affect the sputtering rate.

Hardness and modulus of the coatings as obtained by

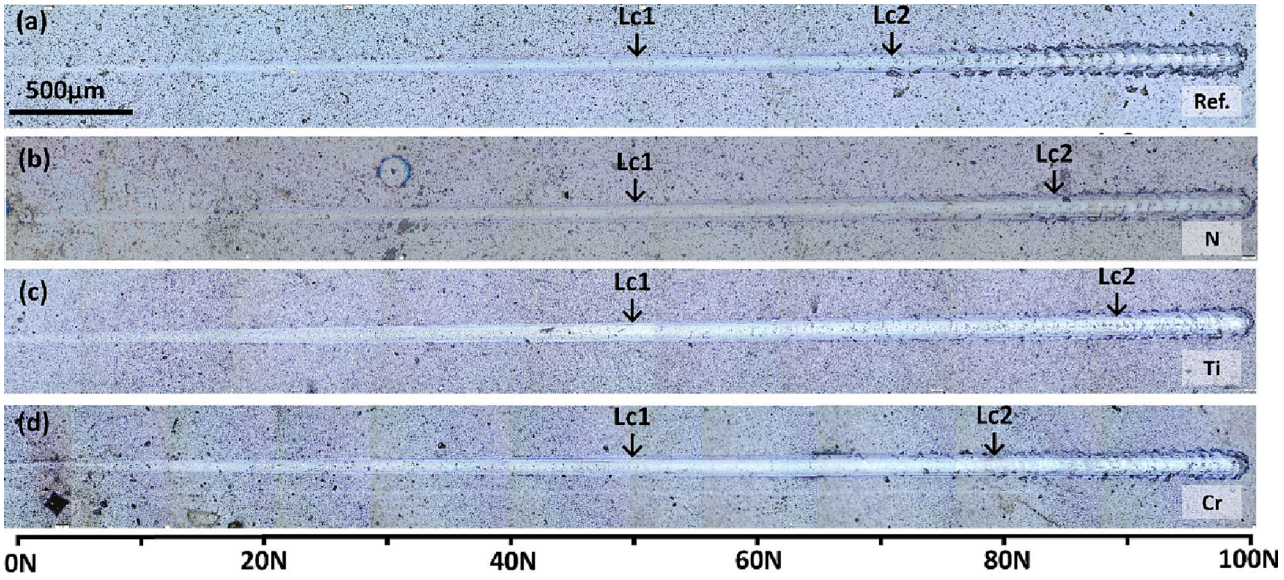

Fig. 9. Optic microscope images of scratch test on each sample, indicating critical loads for samples: (a) Reference AlCrSiN, (b) N/AlCrSiN, (c) Ti/AlCrSiN and (d) Cr/AlCrSiN. It can be observed that Lc2 (spallation of the coating) is higher for coatings with implantation in the substrate.

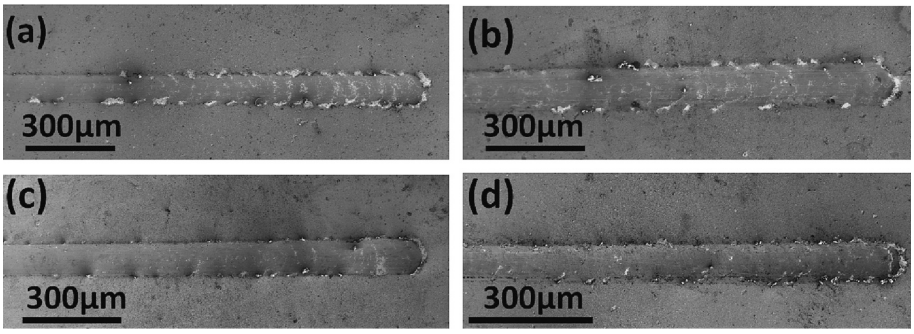

Fig. 10. SEM images of scratch test in: (a) Reference AlCrSiN, (b) N/AlCrSiN, (c) Ti/AlCrSiN and (d) Cr/AlCrSiN. Higher amount of spallation and more substrate exposition (with whiter contrast) is observed for reference and nitrogen implanted samples.

nanoindentation tests were similar to the literature [40] and no significant difference between implanted and non-implanted samples is observed, implying that ion implantation of the substrate does not affect the elastoplastic response of the coating, as expected.

Ion implantation improves the measured apparent fracture toughness of the substrate, due to the introduction of compressive residual stresses, which hinders crack propagation and results in shorter cracks produced by Vickers indentation, as reported by Halitim et al. [18]. This would provide higher toughness of the substrate and may increase local load bearing capacity of the substrate. A higher value of residual stresses is present in the substrates with Ti and Cr implantation.

Calculated residual stresses for the coatings are consistent with the literature, with values ranging between 5 and 6 GPa. In this respect, Korsunsky et al. [33] obtained a residual stress of -6.16 ± 0.53 GPa using ring-core geometry for a TiN coating on WC-Co substrate, and Sebastiani et al. [34] calculated a value of -5.51 ± 0.33 GPa with double slot geometry for a CrN coating on steel substrate. The residual stresses obtained are slightly higher, but are in the same range and negative, indicating that the coating exhibits compressive residual stress.

In the scratch tests it can be clearly observed how ion implantation of the substrate improves the scratch resistance and therefore the adhesion of the coatings, since the L_{c2}, referring to the adhesion strength of the substrate-coating, is higher for the implanted samples. Although the scratch resistance is improved with ion implantation of any of the three studied ions, the Cr and Ti implanted samples show a better response since it can be observed how the coating is not lifted as significantly and considerably less substrate area is exposed, compared to the N-implanted sample and the reference.

Mercedes test results are consistent with scratch test results, where the sample without ion implantation exhibits a larger delamination area, while Ti and Cr samples present a lower delamination area. For Cr/AlCrSiN and Ti/AlCrSiN samples the coating remains attached to the substrate, while in Ref/AlCrSiN and N/AlCrSiN the substrate is exposed, which indicates a better adhesion strength for Ti and Cr implanted samples.

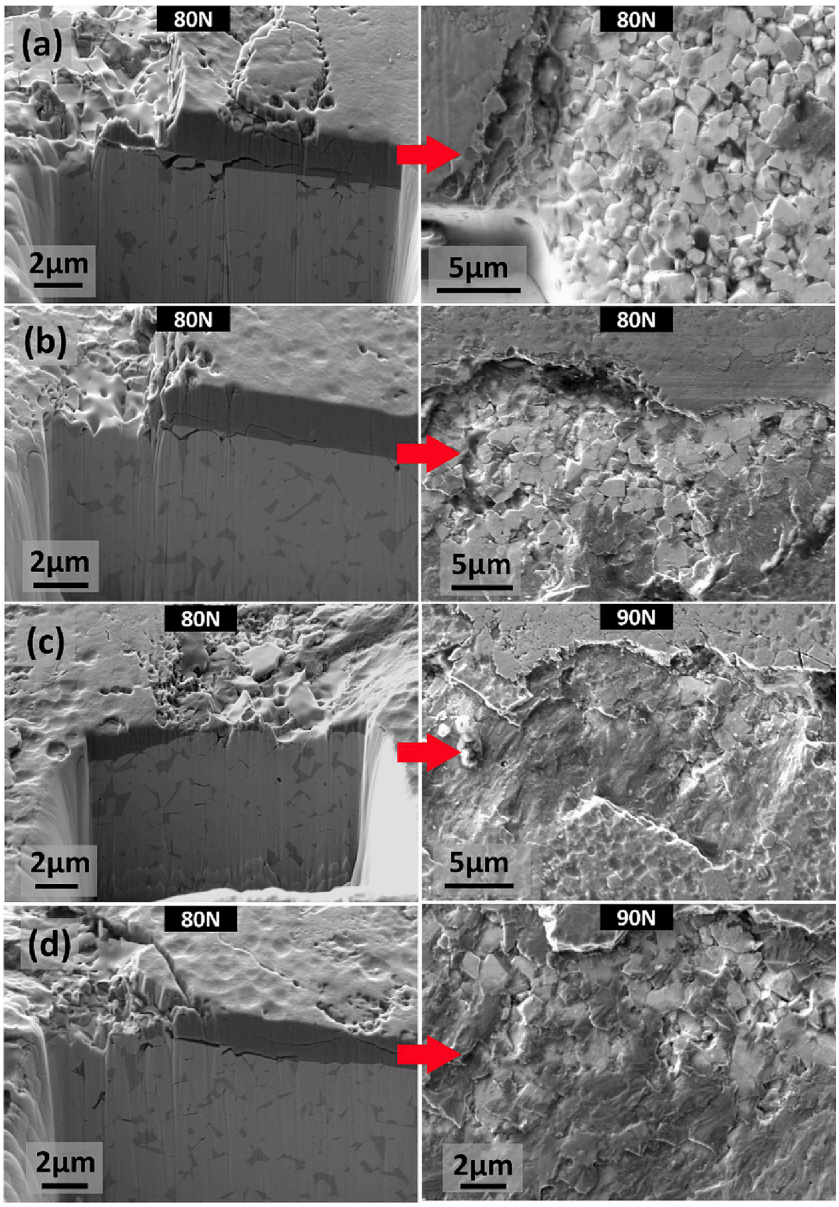

Fig. 11. Cross-sectional SEM images of spallation zones at 80 N and substrate exposure of: (a) Reference AlCrSiN, (b) N/AlCrSiN, (c) Ti/AlCrSiN and (d) Cr/AlCrSiN. In the left are presented the cross sections milled with FIB and in the right surface images. Notice that the samples implanted with Ti and Cr present a fracture near the interface with the coating. The sample implanted with N, as well as the reference presents fracture of the carbides.

The apparent fracture toughness and compressive residual stress of the substrates increase with ion implantation, reaching higher values for Ti and Cr implanted substrates, which may increase the local load bearing capacity of the substrate. This increase prevents the fracture of the cemented carbide grains of the substrate, as is observed in the cross-sectional images in Fig. 11, where a slightly more fractured substrate appears at the same load (80 N) for reference and N implanted coated samples, while in Ti and Cr implanted coated samples, those that exhibit the best adhesion strength, the substrate remains almost intact. While the indentation method may be inaccurate for measuring residual stress produced by ion implantation, other effects may not be discarded. In particular, ion implantation can change the chemistry of the carbides, or diffusion of the implanted ions can occur during coating deposition.

Furthermore, the texture produced by the ion implantation on the substrate surface for the Ti and Cr implanted samples, as shown in Fig. 3, produces a mechanical interlocking between the substrate and the coating, which can be seen in the cross section images in Fig. 7. This mechanical interlocking may be contributing to the improved adhesion for the Ti and Cr implanted samples.

Compressive residual stress introduced into the substrate, promoting a combination of increased indentation fracture toughness and local load bearing capacity of the substrate, together with the mechanical interlocking due to the roughness of the substrate; result in an improvement on the adhesion behaviour of the coated samples. Fig. 13 summarizes the findings in a more visible and graphical manner by connecting the substrate's fracture toughness to the exposed substrate area at 196 N in Mercedes test. The higher substrate toughness and lower substrate exposure area at 196 N in Mercedes test are obtained for Ti/AlCrSiN and Cr/AlCrSiN, the samples that show better adhesion.

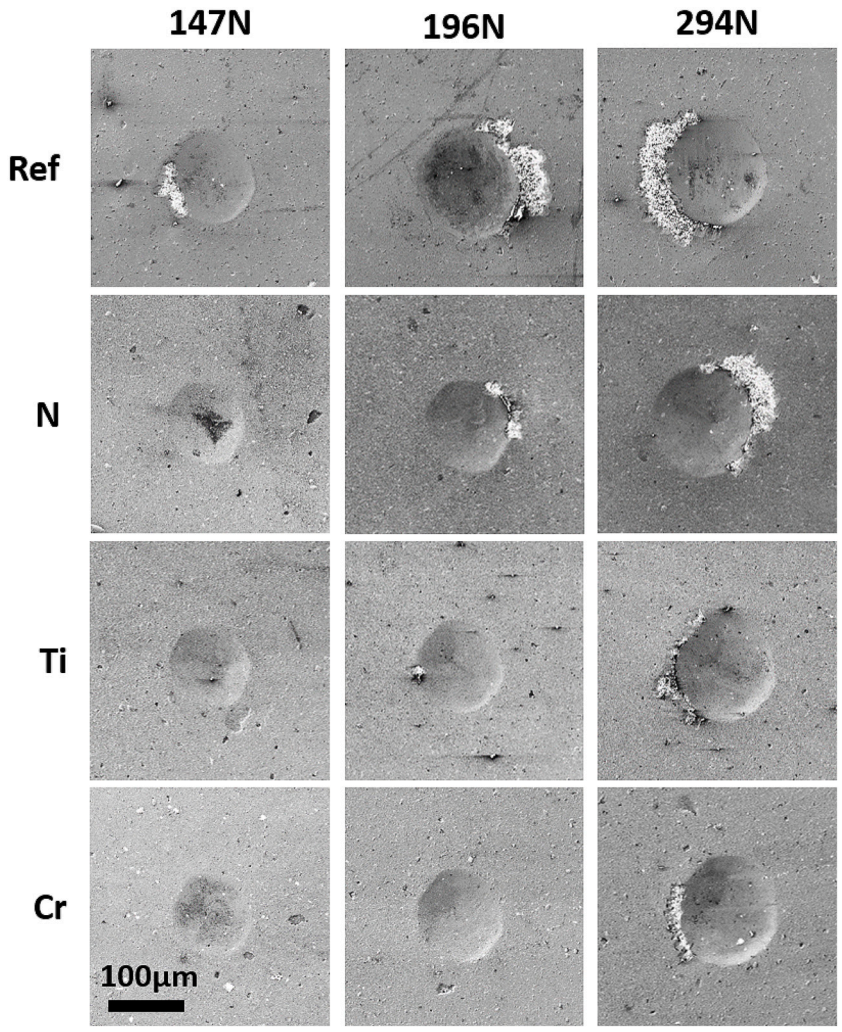

Fig. 12. Optical microscope Rockwell C indentations at different loads in reference AlCrSiN, N/AlCrSiN, Ti/AlCrSiN and Cr/AlCrSiN.

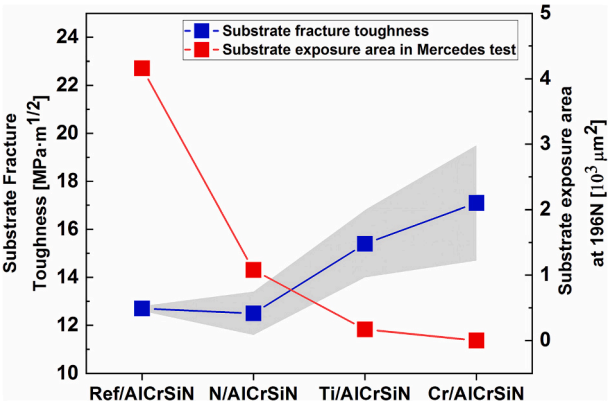

Fig. 13. Representation of measured apparent fracture toughness of the substrate and substrate exposure area at 196 N in the Mercedes test for each sample. Lower substrate exposure area and higher fracture toughness of the substrate are obtained for Ti/AlCrSiN and Cr/AlCrSiN.

5. Conclusions

Nitrogen, titanium and chromium implantation was performed successfully in WC-Co substrates. AlCrSiN coating was deposited on the treated samples.

Ion implantation of the substrate does not seem to modify the mechanical properties of the subsequently deposited coating, nor does affect the residual stress of the coating. All coated samples show the same mechanical properties and residual stresses regardless of ion implantation.

Ion implantation introduces compressive residual stress to the substrate, and therefore the fracture toughness is enhanced.

In the adhesion tests, the results are consistent with each other: it is concluded that Ti and Cr implantation of the substrate improves adhesion of the coatings. This improvement can be related with an apparent increase in fracture toughness of the substrate due to the residual stresses, and the improvement of the local load bearing capacity of the substrate as well as an increase in surface roughness, which produce a mechanical interlocking.

CRediT authorship contribution statement

L. Ortiz-Membrado: Conceptualization, Writing – original draft, Investigation, Visualization. **S. García-González:** Writing – review & editing, Investigation, Visualization. **J. Orrit-Prat:** Writing – review & editing, Investigation. **R. Bonet:** Writing – review & editing, Investigation. **J. Caro:** Conceptualization, Writing – review & editing, Funding acquisition, Investigation. **J. Fernández de Ara:** Conceptualization, Writing – review & editing, Funding acquisition, Investigation. **E. Almandoz:** Conceptualization, Writing – review & editing, Funding acquisition, Investigation. **L. Llanes:** Writing – review & editing, Supervision. **E. Jiménez-Piqué:** Conceptualization, Writing – review & editing, Supervision, Funding acquisition.

Declaration of Competing Interest

The authors declare that they have no known competing financial interests or personal relationships that could have appeared to influence the work reported in this paper.

Data availability

Data will be made available on request.

Acknowledgments

Work funded through The Spanish Ministry of Science, Innovation and Universities through grants PGC-2018-096855-B-C41, PGC-2018-096855-B-C42 and PGC-2018-096855-A-C44.

The authors would like to thank Dr. R. M'Saoubi for kindly providing the

substrates for this research and Metal Estalki for the PVD coating deposition processes.

References

[1] A. Inspektor, P.A. Salvador, Architecture of PVD coatings for metalcutting applications: a review, Surf. Coat. Technol. 257 (2014) 138–153, https://doi.org/10.1016/j.surfcoat.2014.08.068.

[2] A.V. Shatov, S.S. Ponomarev, S.A. Firstov, Fracture and strength of hardmetals at room temperature, in: V.K. Sarin, D. Mari, L. Llanes (Eds.), Comprehensive Hard Materials, Elsevier, UK, 2014, pp. 301–343, https://doi.org/10.1016/B978-0-08-096527-7.00010-6.

[3] P. Kenny, The application of fracture mechanics to cemented tungsten carbides, Powder Metall. 14 (27) (1971) 22–38, https://doi.org/10.1179/pom.1971.14.27.002.

[4] H. Suzuki, K. Hayashi, The strength of WC-Co cemented carbide in relation to structural defects, J. Jpn. Inst. Metals 16 (1974) 354–360, https://doi.org/10.2320/matertrans1960.16.353.

[5] E.A. Almond, B. Roebuck, A. Almond, Defect-initiated fracture and the bend strength of WC-co hardmetals, Metal Sci. 11 (1977) 458–461, https://doi.org/10.1179/msc.1977.11.10.458.

[6] B. Roebuck, E.A. Almond, Deformation and fracture processes and the physical metallurgy of WC-co hardmetals, Int. Mater. Rev. 33 (2) (1988), https://doi.org/10.1179/imr.1988.33.1.90.

[7] J.J. Roa, E. Jiménez-Piqué, R. Martínez, G. Ramírez, J.M. Tarragó, R. Rodríguez, L. Llanes, et al., Contact damage and fracture micromechanisms of multilayered TiN/CrN coatings at micro- and nano-length scales, Thin Solid Films 571 (P2) (2014) 308–315, https://doi.org/10.1016/j.tsf.2014.04.018.

[8] F.O. Ramírez-Reyna, G.A. Rodríguez-Castro, U. Figueroa-López, R.C. Morón, I. Arzate-Vázquez, A. Meneses-Amador, Effect of nitriding pretreatment on adhesion and tribological properties of AlCrN coating, Mater. Lett. 284 (2021), https://doi.org/10.1016/j.matlet.2020.128931.

[9] J.L. Mo, M.H. Zhu, A. Leyland, A. Matthews, Impact wear and abrasion resistance of CrN, AlCrN and AlTiN PVD coatings, Surf. Coat. Technol. 215 (2013) 170–177, https://doi.org/10.1016/j.surfcoat.2012.08.077.

[10] A.Y. Adesina, Z.M. Gasem, A.S. Mohammed, Comparative investigation and characterization of the scratch and wear resistance behavior of TiN, CrN, AlTiN and AlCrN cathodic arc PVD coatings, Arab. J. Sci. Eng. 44 (12) (2019) 10355–10371, https://doi.org/10.1007/s13369-019-04038-8.

[11] Y.X. Wang, S. Zhang, Toward hard yet tough ceramic coatings, Surf. Coat. Technol. 258 (2014) 1–16, https://doi.org/10.1016/j.surfcoat.2014.07.007.

[12] S.J. Suresha, S. Math, V. Jayaram, S.K. Biswas, Toughening through multilayering in TiN-AlTiN films, Philos. Mag. 87 (17) (2007) 2521–2539, https://doi.org/10.1080/14786430701230245.

[13] K. Yalamanchili, F. Wang, H. Aboulfadl, J. Barrirero, L. Rogström, E. Jiménez-Pique, F. Mücklich, F. Tasnadi, M. Odén, N. Ghafoor, Growth and thermal stability of TiN/ZrAlN: effect of internal interfaces, Acta Mater. 121 (2016) 396–406, https://doi.org/10.1016/j.actamat.2016.07.006.

[14] K. Yalamanchili, R. Forsén, E. Jiménez-Piqué, M.P. Johansson Jöesaar, J.J. Roa, N. Ghafoor, M. Odén, Structure, deformation and fracture of arc evaporated Zr-Si-N hard films, Surf. Coat. Technol. 258 (2014) 1100–1107, https://doi.org/10.1016/j.surfcoat.2014.07.024.

[15] Y.X. Wang, S. Zhang, J.W. Lee, W.S. Lew, B. Li, Influence of bias voltage on the hardness and toughness of CrAlN coatings via magnetron sputtering, Surf. Coat. Technol. 206 (24) (2012) 5103–5107, https://doi.org/10.1016/j.surfcoat.2012.06.041.

[16] M. Haršáni, N. Ghafoor, K. Calamba, P. Zacková, M. Sahul, T. Vopát, L. Satrapinskyy, M. Čaplovičová, Ľ. Čaplovič, Adhesive-deformation relationships and mechanical properties of nc-AlCrN/a-SiNx hard coatings deposited at different bias voltages, Thin Solid Films 650 (2018) 11–19, https://doi.org/10.1016/j.tsf.2018.02.006.

[17] O. Abe, Y. Ohwa, Oxidation of $NiAl/Al_2O_3$ composites for controlled development of surface layers and toughening, Solid State Ionics 172 (1–4) (2004) 553–556, https://doi.org/10.1016/j.ssi.2004.02.062. SPEC. ISS.

[18] F. Halitim, N. Ikhlef, L. Boudoukha, G. Fantozzi, Microhardness, Young's modulus and fracture toughness of alumina implanted with Zr+, Cr+, Ti+ and Ni+. The effect of the residual stresses, J. Phys. D. Appl. Phys. 30 (3) (1997) 330–337, https://doi.org/10.1088/0022-3727/30/3/004.

[19] K. Weng, Y. Chen, T. Lin, D. Wang, Characterization of titanium nitride coatings deposited by metal plasma ion pre-implantation and cathodic arc evaporation, J. Nanosci. Nanotechnol. 9 (2) (2009) 1127–1132, https://doi.org/10.1166/jnn.2009.C102.

[20] P.W. Shum, Y.F. Xu, Z.F. Zhou, K.Y. Li, Effects of carbon and nitrogen ion implantations on surface and tribological properties of Ti – Al – Si – N coatings, in: Special Issue Article from Asia Pacific Interfinish 2010 – 10th International Conference on Applied Surface Engineering 28, 2012, pp. 149–155, https://doi.org/10.1179/1743294411Y.0000000071, no. 2.

[21] S. Ulrich, H. Holleck, J. Ye, H. Leiste, R. Loos, M. Stüber, P. Pesch, S. Sattel, Influence of low energy ion implantation on mechanical properties of magnetron sputtered metastable (Cr,Al)N thin films, Thin Solid Films 437 (1–2) (2003) 164–169, https://doi.org/10.1016/S0040-6090(03)00595-9.

[22] Y. Liu, L. Li, X. Cai, Q. Chen, M. Xu, Y. Hu, T.-L. Cheung, C.C. Shek, P.K. Chu, Effects of pretreatment by ion implantation and interlayer on adhesion between aluminum substrate and TiN film, Thin Solid Films 493 (1–2) (2005) 152–159, https://doi.org/10.1016/j.tsf.2005.06.045.

[23] L. Wang, L. Li, G. Li, Improved adhesion of TiAlSiN nanocomposite coatings on cemented carbide substrate by pre-implantation, Coatings 9 (3) (2019) 209, https://doi.org/10.3390/COATINGS9030209.

[24] J.L. Mosquera, L. Mera, G.S. Fox-Rabinovich, R. Martínez, I. Azkona, J.L. Endrino, Advantages of Nanoimpact fracture testing in studying the mechanical behavior of CrAl(Si)N coatings, Nanosci. Nanotechnol. Lett. 2 (2010), https://doi.org/10.1166/nnl.2010.1108.

[25] K. Niihara, R. Morena, D.P.H. Hasselman, Indentation fracture toughness of brittle materials for Palmqvist cracks, in: R.C. Bradt, A.G. Evans, D.P.H. Hasselman, F. F. Lange (Eds.), Fracture Mechanics of Ceramics vol., 5, 1982, pp. 97–105. Plenum, NY.

[26] K. Niihara, A fracture mechanics analysis of indentation-induced Palmqvist crack in ceramics, J. Mater. Sci. Lett. 2 (1983) 221–223, https://doi.org/10.1007/BF00725625.

[27] D.J. Green, B. Maloney, Influence of surface stress on indentation cracking, J. Am. Ceram. Soc. 69 (1986) 223–225, https://doi.org/10.1111/j.1151-2916.1986.tb07412.x.

[28] G. de Portu, S. Conoci, Simplified equation for evaluating the influence of surface residual stresses on the toughness of zirconia ceramics, J. Am. Ceram. Soc. 80 (1997) 3242–3244, https://doi.org/10.1111/j.1151-2916.1997.tb03260.x.

[29] W. Oliver, G. Pharr, An improved technique for determining hardness and elastic modulus using load and displacement sensing indentation experiments, J. Mater. Res. 7 (6) (1992) 1564–1583, https://doi.org/10.1557/JMR.1992.1564.

[30] C.A. Botero, E. Jimenez-Piqué, J. Seuba, T. Kulkarni, V.K. Sarin, L. Llanes, Mechanical behavior of $3Al_2O_3{\cdot}2SiO_2$ films under nanoindentation, Acta Mater. 60 (16) (2012) 5889–5899, https://doi.org/10.1016/j.actamat.2012.07.031.

[31] M. Sebastiani, E. Rossi, M. Zeeshan Mughal, A. Benedetto, P. Jacquet, E. Salvati, A. M. Korsunsky, Nano-scale residual stress profiling in thin multilayer films with non-equibiaxial stress state, Nanomaterials 10 (no 5) (2020), https://doi.org/10.3390/nano10050853.

[32] M. Sebastiani, C. Eberl, E. Bemporad, G.M. Pharr, Depth-resolved residual stress analysis of thin coatings by a new FIB-DIC method, Mater. Sci. Eng. A 528 (27) (2011) 7901–7908, https://doi.org/10.1016/j.msea.2011.07.001.

[33] A.M. Korsunsky, M. Sebastiani, E. Bemporad, Residual stress evaluation at the micrometer scale: analysis of thin coatings by FIB milling and digital image correlation, Surf. Coat. Technol. 205 (7) (2010) 2393–2403, https://doi.org/10.1016/j.surfcoat.2010.09.033.

[34] M. Sebastiani, C. Eberl, E. Bemporad, A.M. Korsunsky, W.D. Nix, F. Carassiti, Focused ion beam four-slot milling for Poisson's ratio and residual stress evaluation at the micron scale, Surf. Coat. Technol. 251 (2014) 151–161, https://doi.org/10.1016/j.surfcoat.2014.04.019.

[35] M. Krottenthaler, C. Schmid, J. Schaufler, K. Durst, M. Göken, A simple method for residual stress measurements in thin films by means of focused ion beam milling and digital image correlation, Surf. Coat. Technol. 215 (2013) 247–252, https://doi.org/10.1016/j.surfcoat.2012.08.095.

[36] J. Lord, D. Cox, A. Ratzke, A good practice guide for measuring residual stresses using FIB-DIC, in: Good Practice Guide vol. 143, 2018, https://doi.org/10.1093/acprof:oso/9780198565932.003.0002.
[37] A. C1624—05, Standard test method for adhesion strength and mechanical failure modes of, ASTM Int. C1624–05 (2015) 1–29, https://doi.org/10.1520/C1624-05R10.Scope, no. Reapproved 2010.
[38] N. Vidakis, A. Antoniadis, N. Bilalis, The VDI 3198 indentation test evaluation of a reliable qualitative control for layered compounds, J. Mater. Process. Technol. 143–144 (1) (Dec. 2003) 481–485, https://doi.org/10.1016/S0924-0136(03)00300-5.
[39] B.R. Lawn, E.R. Fuller, Measurement of thin-layer surface stresses by indentation fracture, J. Mater. Sci. 19 (1984) 4061–4067, https://doi.org/10.1007/BF00980772.
[40] T. Sampath Kumar, S. Balasivanandha Prabu, G. Manivasagam, K. A. Padmanabhan, Comparison of TiAlN, AlCrN, and AlCrN/TiAlN coatings for cutting-tool applications, Int. J. Miner. Metall. Mater. 21 (8) (2014) 796–805, https://doi.org/10.1007/s12613-014-0973-y.